

UL-NTZ 19/98  
KANAZAWA-98-09

# Wave Functions and Spectrum in Hot Electroweak Matter for Large Higgs Masses

E.-M. Ilgenfritz<sup>1\*</sup>, A. Schiller<sup>2†</sup>, and C. Strecha<sup>2‡</sup>

<sup>1</sup> *Institute for Theoretical Physics, Kanazawa University,  
Kanazawa 920, Japan*

<sup>2</sup> *Institut für Theoretische Physik and NTZ,  
Universität Leipzig, Germany*

July 10, 1998

## Abstract

We present results for the wave functions and the screening mass spectrum for quantum numbers  $0^{++}$ ,  $1^{--}$  and  $2^{++}$  in the three-dimensional  $SU(2)$ –Higgs model near to the phase transition line below the endpoint and in the crossover region. Varying the  $3D$  gauge couplings we study the behaviour along a line of constant physics towards the continuum limit in both phases. In the crossover region the changing spectrum of screening states versus temperature is examined showing the aftermath of the phase transition at lower Higgs mass. Different to smearing concepts we used large sets of operators with various extensions allowing to identify wave functions in position space.

## 1 Introduction

During last years, due to efforts of three groups [1]–[5] using the  $3D$  approach, various aspects of the high temperature electroweak phase transition have been explored in the  $SU(2)$ –Higgs model, increasing the Higgs mass  $M_H$  from light to heavy. When one comes near to the  $W$  mass  $M_W$  the character of the transition is known to change drastically. The interface tension has been seen falling over three orders of magnitude [1, 6] (if expressed as  $\alpha/T_c^3$ ), whereas the latent heat goes to zero roughly linearly. The continuum characteristics of the transition cannot be determined with the same precision by  $4D$

---

\*ilgenfri@hep.s.kanazawa-u.ac.jp

†schiller@tph204.physik.uni-leipzig.de

‡strecha@tph204.physik.uni-leipzig.de

Monte Carlo simulations [7], although the results are consistent with each other where they can be compared [8, 6].

The 4D lattice approach meets two problems which made the 3D approach so attractive. At first, only the bosonic sector can be studied because of the problems to deal with chiral fermions. Second, simulations are difficult due to the different length scales. The inverse Matsubara frequency,  $1/(2\pi T)$ , is much shorter than the two correlation lengths,  $1/m_W(T)$  and  $1/m_H(T)$ , with the screening masses differing strongly from the zero temperature masses. If the temporal lattice extent  $N_\tau$  should be not too small, they can be accommodated on a 4D lattice only if this is anisotropic. This requires more couplings to be tuned than in the isotropic case when one first has to match the  $M_H/M_W$  ratio and the renormalised coupling  $g_4^2(\mu_4)$  on a  $T = 0$  ( $N_\tau = N_s$ ) lattice.

The 3D approach represents itself as a radical solution to both problems. It is based on perturbative dimensional reduction in the continuum combined with lattice perturbation theory [9], leaving to lattice simulation only the non-perturbative description of the softest modes whose behaviour governs the transition. All non-zero Matsubara modes are integrated out leaving an effective, superrenormalisable theory in 3D with the smallest length scale  $1/(2\pi T)$  removed. Chiral fermions can be implicitly included at this step. In a second step the next heaviest modes related to the Debye mass  $m_D \sim g T$  (the  $A_0$  components of the gauge field) are integrated out. Thus an effective 3D  $SU(2)$ –Higgs theory emerges with the action

$$S_3 = \int d^3x \left( \frac{1}{4} F_{\mu\nu}^b F_{\mu\nu}^b + (D_\mu \phi)^+ (D_\mu \phi) + m_3^2 \phi^+ \phi + \lambda_3 (\phi^+ \phi)^2 \right). \quad (1)$$

It has dimensionful, renormalisation group invariant couplings  $g_3^2$  and  $\lambda_3$  and a running mass squared  $m_3^2(\mu_3)$ . It is put into correspondence to the lattice model with the action

$$S = \beta_G \sum_p (1 - \frac{1}{2} \text{tr} U_p) - \beta_H \sum_{x,\mu} \frac{1}{2} \text{tr} (\Phi_x^+ U_{x,\mu} \Phi_{x+\hat{\mu}}) + \sum_x (\rho_x^2 + \beta_R (\rho_x^2 - 1)^2). \quad (2)$$

The lattice couplings are (with a suitable parameter  $M_H^*$ )

$$\begin{aligned} \beta_G &= \frac{4}{a g_3^2}, \quad \beta_R = \frac{\lambda_3 \beta_H^2}{g_3^2 \beta_G} = \frac{1}{8} \left( \frac{M_H^*}{80 \text{ GeV}} \right)^2 \frac{\beta_H^2}{\beta_G}, \\ \beta_H &= \frac{2(1 - 2\beta_R)}{6 + a^2 m_3^2}, \end{aligned} \quad (3)$$

which can be expressed in terms of 4D couplings and masses. The parameter  $M_H^*$  is approximately equal to the zero temperature physical Higgs mass. The summation in (2) is taken over plaquettes  $p$ , sites  $x$  and links  $l = \{x, \mu\}$ . The gauge fields are represented by unitary  $2 \times 2$  link matrices  $U_{x,\mu}$  and  $U_p$  denotes the  $SU(2)$  plaquette matrix. The Higgs field is parametrised as follows:  $\Phi_x = \rho_x V_x$ , where  $\rho_x^2 = \frac{1}{2} \text{tr} (\Phi_x^+ \Phi_x)$  is the Higgs modulus squared, and  $V_x$  an element of the group  $SU(2)$ .

The bare mass squared is related to the renormalised  $m_3^2(\mu_3)$  (we choose  $\mu_3 = g_3^2$ ) through a lattice two-loop calculation [10] giving  $m_3^2(\mu_3) = m_3^2 + m_{1\text{-loop}}^2 + m_{2\text{-loop}}^2$ . The lattice results obtained in the 3D approach indicate the validity of the dimensional reduction (without additional operators in the action) near to the transition temperature for

Higgs masses in the range between 30 and 240 GeV. The relations between the parameters of the effective  $3D$  model and the physical quantities Higgs mass and temperature are derived in [9].

According to recent lattice studies [4, 5, 11] the standard electroweak theory ceases to possess a first order transition for a Higgs mass  $M_H > 72$  GeV. Therefore, taking the newest lower bound of the Higgs mass into account [12], it has become very likely that the standard model does not pass through a true phase transition at the electroweak vector boson mass scale. This and the small amount of CP violation in the standard model seem to rule out the possibility to explain the BAU generation without new physics. Therefore the phenomenological interest has moved to extensions of the standard model, with minimal supersymmetric extensions (MSSM) being the most promising variant. First interesting lattice results have been published recently [13].

From the point of view of non-perturbative physics in general, the lattice version of the standard Higgs model is still interesting as a laboratory for investigating the behaviour of hot gauge fields coupled to scalar matter, for the characterisation of possible bound states, for the understanding of real time topological transitions and the influence of embedded topological defects [14] on the transition. It has played an important role as a cross-check for analytical approximation schemes and will do so in future.

We are concentrating in this paper on the qualitative change of the spectrum of screening states that happens across the phase transition and what remains of it in the crossover region (at slightly higher Higgs mass). This would not be possible without a systematic evaluation of the wave functions in configuration space that, for the first time in this context, is attempted here. Some intermediate results have been published before [15].

The rest of this paper is organised as follows. In Sect. 2 we discuss the cross correlation technique and the operator set as we have used them. The wave functions and masses of the ground state and excited states near to the endpoint of the phase transition are presented in Sects. 3 and 4 for the symmetric and the Higgs phase at  $M_H^* = 70$  GeV, respectively. This complements a recent study in [16] which has been performed, however, at much lighter ( $M_H^* = 35$  GeV) Higgs mass. Section 5 contains our results for the dynamics of the spectrum with increasing temperature in the crossover region for  $M_H^* = 100$  GeV, slightly above the first order endpoint which can be compared with results of [17] at a clearly larger Higgs mass  $M_H^* \approx 120$  GeV. In Sect. 6 we summarise our results. The Appendices contain tables of the measured mass values obtained from this analysis and details how to construct the operator set for the quantum numbers in  $2+1$  dimensions on the lattice.

## 2 The Cross Correlation Technique in the $3D$ Model

To study simultaneously the ground state and excited states (and possibly their wave functions) one has to consider cross correlations between operators  $\mathcal{O}_i$  from a complete set in a given  $J^{PC}$  channel with quantum numbers  $J$  (angular momentum),  $P$  (parity) and  $C$  (charge conjugation). According to the transfer matrix formalism, one should be able to write the connected correlation matrix at time separation  $t$  in the spectral

decomposition form

$$C_{ij}(t) = \sum_{n=1}^{\infty} \Psi_i^{(n)} \Psi_j^{(n)*} e^{-m_n t} \quad (4)$$

with

$$\Psi_i^{(n)} = \langle \text{vac} | \mathcal{O}_i | \Psi^{(n)} \rangle \quad (5)$$

where  $|\Psi^{(n)}\rangle$  is the  $n$ -th (zero momentum) energy eigenstate. The vacuum state is dropped from this sum due to the connectedness. By suitable diagonalisation this allows to find masses *and* wave functions of the lowest mass screening states (ground state) and higher mass excited states in the various  $J^{PC}$  channels.

However, in practice one has to choose a truncated set of operators  $\mathcal{O}_i$ , ( $i = 1, \dots, N$ ). The hope is that the lowest lying states ( $k = 1, \dots, r$ , with  $r \ll N$ ) might not be essentially affected by the truncation and that their masses and wave functions can be approximately extracted from the direct eigenvalue problem for  $C_{ij}(t)$

$$\sum_j C_{ij}(t) \Psi_j^{(n)} = \lambda^{(n)}(t) \Psi_i^{(n)}. \quad (6)$$

Experience shows that this solution suffers from big systematic truncation errors. Solving instead the generalised eigenvalue problem

$$\sum_j C_{ij}(t) \Psi_j^{(n)} = \lambda^{(n)}(t, t_0) \sum_j C_{ij}(t_0) \Psi_j^{(n)} \quad (7)$$

or

$$\sum_j \tilde{C}_{ij}(t, t_0) \tilde{\Psi}_j^{(n)} = \lambda^{(n)}(t, t_0) \tilde{\Psi}_i^{(n)}, \quad (8)$$

with

$$\tilde{C}_{ij}(t, t_0) = \left( C^{-\frac{1}{2}}(t_0) C(t) C^{-\frac{1}{2}}(t_0) \right)_{ij}, \quad (9)$$

( $t > t_0$ , where practically  $t_0 = 0, 1, \dots$ ) errors related to this truncation can be kept minimal [18, 19]. Practically the decomposition of the matrix  $C(t_0)$  is performed using a Cholesky decomposition  $C(t_0) = LL^T$ . The remaining problem is that of a symmetric matrix  $\tilde{C}(t, t_0) = L^{-1}C(t)L^{-T}$  with rotated eigenvectors  $\tilde{\Psi}^{(n)} = L^T \Psi^{(n)}$ .

The optimised eigenfunctions  $\Psi^{(n)}$  in the chosen operator basis (obtained with a small distance  $t_0$ ) give an information about the overlap of the source operators  $\mathcal{O}_i$  with the actual eigenstates  $|\Psi^{(n)}\rangle$ . Due to truncation the eigenvectors of (7) are not supposed to be orthogonal to each other since  $C^{-1}(t_0)C(t)$  is not a symmetric matrix. The components of the eigenvectors  $\Psi_k^{(n)}$  ( $n \leq N$ ) are effected by terms of the order  $O(\exp(-m_{N+1}t))$ , where  $N$  is the number of used operators. Only in the limit of a complete set of operators the eigenvectors become orthogonal. Therefore, the (non)orthogonality between different states provides a criterion for the completeness of the operator set.

The masses  $m^{(n)}$  of these states are obtained by fitting not the eigenvalues  $\lambda^{(n)}$  of (8) but the diagonal elements  $\mu^{(n)}$

$$\mu^{(n)}(t, t_0) = \sum_{ij} \tilde{\Psi}_i^{(n)} \tilde{C}_{ij}(t, t_0) \tilde{\Psi}_j^{(n)} \quad (10)$$

to a  $\cosh$  form with  $t$  in some plateau region of a local effective mass

$$m_{\text{eff}}^{(n)}(t, t_0) = \log \frac{\mu^{(n)}(t, t_0)}{\mu^{(n)}(t + 1, t_0)}. \quad (11)$$

The wave function components with respect to the operator basis characterise the coupling of source operators  $\mathcal{O}_i$  to the bound states (lowest mass or excited) in the  $J^{PC}$  channel. Using operators of different extension transverse to the correlation direction a spatial resolution of the optimised wave function can be achieved. Practically only a subset of operators with fixed quantum numbers can be included. The admitted operator set includes gauge invariant operators properly chosen with respect to the lattice symmetry and quantum numbers. For completeness, the choice of the gauge invariant operators in 2 + 1 dimensions on the cubic lattice corresponding to the quantum numbers mentioned is discussed in Appendix B. Though the results might be in principle known a reasonable presentation for the lattice  $SU(2)$ –Higgs model similar to that of [23] for 3+1 dimensions was not available.

In order to associate a spatial structure to the states under study one has to use operators which correspond to various extension. One way is to define a set of operators using smearing techniques in several variants. In the present context this has been used in [20, 16, 17], using smearing of gauge links and Higgs fields. The smearing parameter determines a well-defined mixture of various lengths in the source operator and has to be optimised by a variational procedure (strictly speaking, for all states separately).

In contrast to this smearing technique, we have chosen the other extreme and collected only a few types of operators  $\mathcal{O}_i$  into our base (properly chosen with respect to lattice symmetry and quantum numbers) but with a wide span of sizes  $l$  in lattice spacings. Such a basis allows to obtain information on the spatial extension of a bound state without going through a variational procedure (for the lowest and the excited states). In principle, now a smearing of link and Higgs variables underlying these operators would be conceivable for further optimising the states under study. We have restricted ourselves to the varying spatial extent.

In the three quantum number channels investigated here we have admitted the following operators (with  $\mu = 3$  used as correlation direction, see Appendix B):

$$\begin{aligned} 0^{++} : \quad & \rho_x^2 \\ & S_{x,1}(l) + S_{x,2}(l) \\ & W_{x,1,2}(l) + W_{x,1,2}(l) \quad \text{quadratic Wilson loops of size } l \times l \\ 1^{--} : \quad & V_{x,1}^b(l) + V_{x,2}^b(l) \\ 2^{++} : \quad & S_{x,1}(l) - S_{x,2}(l) \end{aligned} \quad (12)$$

Here the following notation is used ( $l$  counts the string length in lattice units)

$$S_{x,\mu}(l) = \frac{1}{2} \text{tr}(\Phi_x^+ U_{x,\mu} \dots U_{x+(l-1)\hat{\mu},\mu} \Phi_{x+l\hat{\mu}}), \quad (13)$$

$$V_{x,\mu}^b(l) = \frac{1}{2} \text{tr}(\tau^b \Phi_x^+ U_{x,\mu} \dots U_{x+(l-1)\hat{\mu},\mu} \Phi_{x+l\hat{\mu}}). \quad (14)$$

Since already the masses of the lowest states in the  $2^{++}$  channel are relatively heavy we have not included Wilson loop contributions here. Therefore, the information about  $2^{++}$  excited states has to be taken with care.

In our procedure, finding the eigenfunctions  $\tilde{\Psi}_i^{(n)}$  is tantamount to determine an optimal source operator  $\mathcal{O}^{(n)}$  for the eigenstate  $|\Psi^{(n)}\rangle$  as a superposition of the original operators  $\mathcal{O}_i$ ,

$$\mathcal{O}^{(n)} = \sum_{i=1}^N \Psi_i^{(n)} \mathcal{O}_i, \quad (15)$$

where the coefficients  $\Psi_i^{(n)}$  are related to the normalised solutions  $\tilde{\Psi}_i^{(n)}$  of the generalised eigenvalue equation (8) by  $\Psi_i^{(n)} = C^{-1/2}(t_0)_{ij} \tilde{\Psi}_j^{(n)} / (\mu^{(n)}(t_0, t_0))^{1/2}$ . These coefficients define the weight of the chosen operators to the operator  $\mathcal{O}^{(n)}$  and express the spatial extendedness of the eigenstate  $|\Psi^{(n)}\rangle$  under study.

Later on, in the  $1^{--}$  and  $2^{++}$  channels the index  $i$  is used to label the size  $l$  of the corresponding operator in lattice units. In the case of the  $0^{++}$  channel the label  $l = 0$  refers to the operator  $\rho_x^2$ , and for  $l \geq 1$  we have to discriminate between the contributions from links and from Wilson loops.

We have performed simulations using the update algorithms as described in our previous works [3]. In the error analysis of the wavefunctions and masses we have used the jackknife technique. As an example of the outcome of the analysis we show in Fig. 1 the

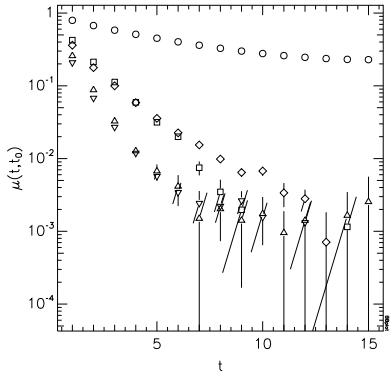


Figure 1: Example of the exponential decay of  $\mu^{(n)}(t, t_0)$  for the 5 lowest states

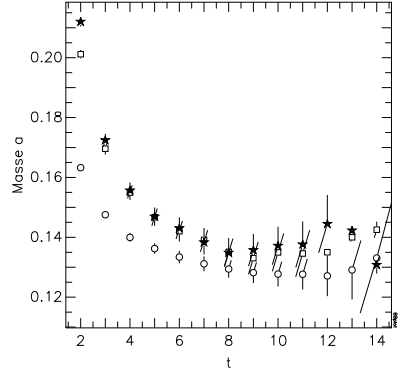


Figure 2:  $0^{++}$  ground state effective mass obtained from cross correlations ( $\circ$ ), compared to results solely from  $S_{x,1} + S_{x,2}$  ( $\square$ ) and  $\rho_x^2$  ( $\star$ ).

exponential decay of the diagonal elements of the correlation matrix  $\mu^{(n)}(t, t_0)$  for the first five states ( $n = 1, \dots, 5$ ) in the symmetric phase ( $\beta_G = 12, \beta_H = 0.3434$ ) at a Higgs mass of  $M_H^* = 70$  GeV in the  $0^{++}$  channel. The mass estimates are obtained by fitting a plateau region to  $\cosh$  taking into account the estimated errors on the correlation functions. The improvement achieved by using cross correlations is demonstrated in Fig. 2. As expected, the cross correlation method leads to lower mass values.

The measurements for a Higgs mass  $M_H^* = 70$  GeV ( $\lambda_3/g_3^2 \approx 0.09570$ ) were performed below but near to the endpoint of the phase transition. At both sides, in the symmetric and in the Higgs phase, we used lines of constant physics at  $m_3^2(g_3^2)/g_4^2 \approx 0.00023$  in the

symmetric and  $m_3^2(g_3^2)/g_4^2 \approx -0.043$  in the Higgs phase, corresponding to  $T \approx 1.02T_c$  and  $T \approx 0.98T_c$ , respectively [9, 3]. The gauge coupling  $\beta_G$  has been varied from 8 to 16 to allow for an extrapolation to the continuum. The choice of the actual simulation parameters as near as possible to the phase transition line was dictated by the condition to avoid tunnelling between the phases. Besides the used lattice size of  $30^3$  we have additionally investigated the wave functions in the symmetric phase for the  $1^{--}$  and  $2^{++}$  channels on a  $50^3$  lattice which permitted to increase the range of  $l$  in the operator basis. On a lattice of given size, the spatial extension of operators had to be restricted to half of the lattice size.

At the larger Higgs mass of  $M_H^* = 100$  GeV ( $\lambda_3/g_3^2 \approx 0.1953$ ), above the endpoint of the phase transition [4, 5], we have studied the spectral change with decreasing temperature (increasing  $\beta_H$ ) from the "symmetric" to the "Higgs" side of the crossover line at one fixed  $\beta_G = 12$ .

The accumulated statistics of our measurements in the symmetric and Higgs phases as well as in the crossover region for each pair of  $\beta_G$  and  $\beta_H$  values is summarised in Table 1. By measuring the autocorrelations for the operators of interest we determined the

Phase	Channel	$M_H^*$ GeV	$L^3$	$\beta_G$	independent configurations
symmetric	$1^{--}, 2^{++}$	70	$50^3$	8,12,16	20000
	$0^{++}, 1^{--}, 2^{++}$	70	$30^3$	8,12,16	12000
Higgs	$0^{++}, 1^{--}, 2^{++}$	70	$30^3$	8,12,16	12000
crossover	$0^{++}, 1^{--}, 2^{++}$	100	$30^3$	12	4000

Table 1: *Used statistics in the measurements*

frequency of measurements during the updating to obtain independent configurations.

### 3 Bound States in the Symmetric Phase at $M_H^* = 70$ GeV

Using the cross correlation technique we are able to obtain the wave function squared corresponding to the optimised operator for each individual state in the spectrum. Being functions of the physical size, the squared wave functions are shown immediately *vs.*  $l/a g_3^2$  in order to overlay data from measurements at various gauge couplings (lattice spacings) taken along a line of constant physics.

The results for the  $0^{++}$  channel are collected in Figs. 3-5 for the squared wave functions. The contributions from the Higgs and Wilson operators are shown separately to identify clearly Higgs and  $W$ -ball excitations. We observe no mixing of these two operator types in the Higgs ground state and the first excitation. The second excited state in this channel consists of a pure excitation gauge degrees of freedom (d.o.f.) excited and can be identified with a  $W$ -ball in analogy with the glueballs of pure  $SU(2)$ . Our results on

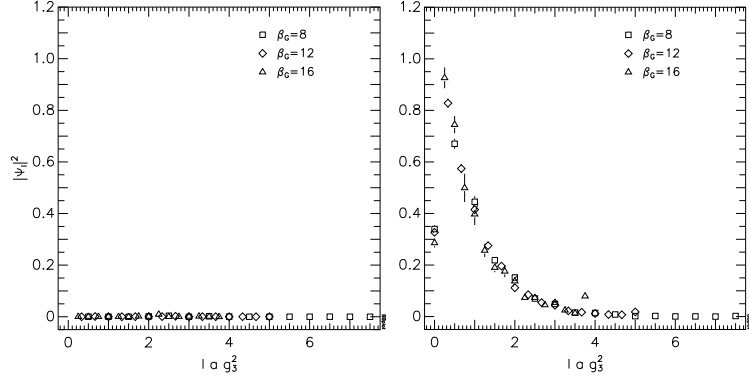


Figure 3: Squared wave function for the ground state in  $0^{++}$  channel, measured on a  $30^3$  lattice in the symmetric phase; left: Wilson loops, right:  $S_{x,\mu}(l)$   $l = 0, \dots, 15$

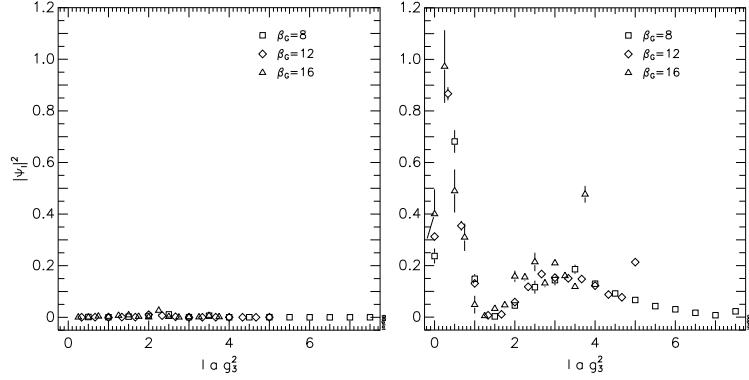


Figure 4: Same as Fig. 3 for the first excited state

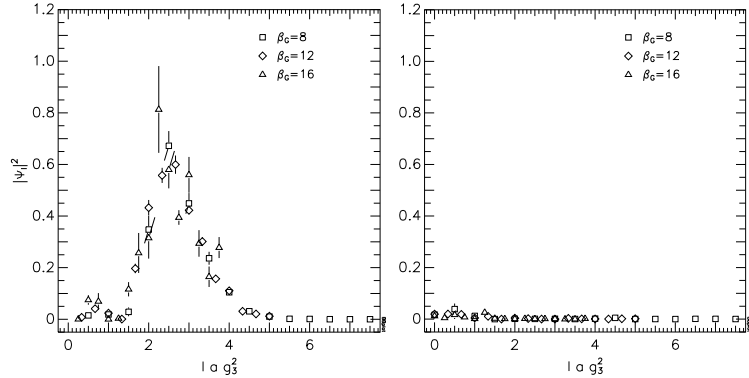


Figure 5: Same as Fig. 3 for the second excited state

this decoupling confirm the observations in [16] made at a much lighter Higgs mass in the symmetric phase near the strongly first order phase transition.

The squared wave functions for ground and excited states in the  $1^{--}$  and  $2^{++}$  channels are presented in Fig. 6 and 7.

At this point it is useful to come back to the issues of completeness of the operator set and of orthogonality of the states  $\Psi_i^{(n)}$ . We have already noticed that the eigenvectors

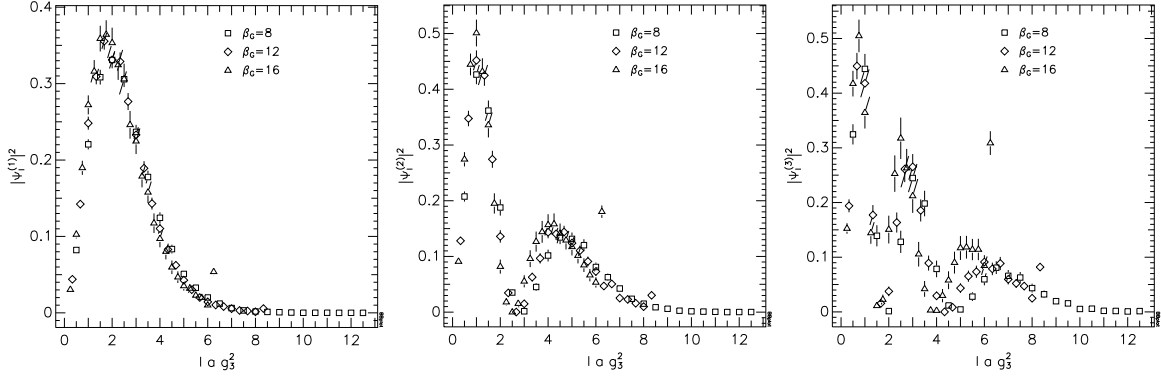


Figure 6: Squared wave function of  $1^{--}$  channel: symmetric phase at  $50^3$  lattice, ground state and two excited states

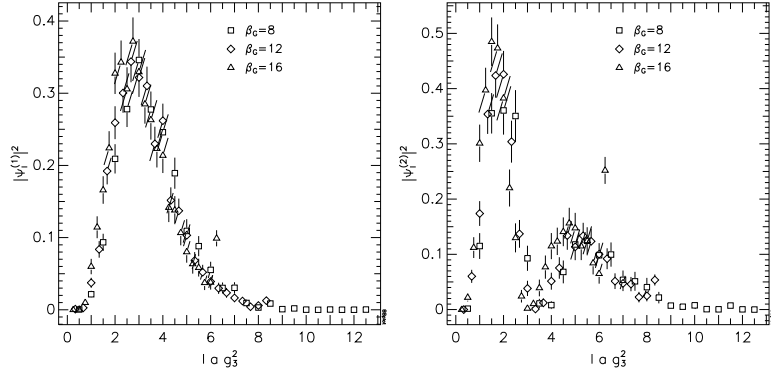


Figure 7: Squared wave function of  $2^{++}$  channel: symmetric phase at  $50^3$  lattice, ground and first excited state

of (7) become orthogonal only in the limit of a complete operator set, and that the scalar product between different states should be used to test the degree of completeness. However, this is difficult in practice. We have studied the scalar product between the ground state and the first excitation as a function of the maximal length  $l_{max}$  of the operator set  $S_{x,\mu}(l)$  by gradually clipping the set of operators from  $l_{max}=25$  (on the  $50^3$  lattice) down to zero. One would expect that this function tends to zero for  $l_{max} \rightarrow \infty$ . Actually the scalar product reaches a minimum at some point and rises at bigger  $l_{max}$  again due to statistical and numerically errors for larger operators and matrices.

Inspecting the wave function of the ground state in the  $1^{--}$  channel we observe that for very large operators the contribution to this state vanishes. This is true to a high accuracy for the largest physical volume that we have considered, at  $\beta_G = 8$ . If we chose higher  $\beta_G$  (smaller volumes) along the line of constant physics (in order to explore the correct continuum behaviour) the operator set in use with  $l_{max} = L/2$  does not describe anymore the whole wave function. There are still fake contributions accumulating in the contribution attributed to the longest operator in the set which should belong to more extended operators. A similar behaviour can be seen in the excited states as well by comparing with a smaller operator set. For the second excited state shown in Fig. 6 it is clearly seen that in the case of  $\beta_G=16$  (small physical volume) this state is not satisfactorily

described by the fixed operator basis. An optimal continuum limit for the wave function would require to choose the same maximal operator length in physical units, *i.e.* doubling the length in lattice units when one goes over from  $\beta_G = 8$  to  $\beta_G = 16$ . This is, however, difficult to realize with restricted resources, not only because of the lattice size. Larger cross correlation matrices would additionally require larger statistics to get stable results from the diagonalisation procedure. Looking for data obtained at fixed  $\beta_G$  (accepting a non-perfect overlay of data in a physical scale) the presented figures illustrate perfectly that the number of zeroes of the wave functions corresponds to the level of excitation (knot rule).

Due to the mentioned difficulties the extraction of higher excitation masses becomes more and more difficult, especially if already the ground state is very heavy, the lattice spacing becomes small (when we attempt to study the continuum limit) and when the wave function has a large physical extension.

For the ground states we are now able to test our previous spectrum investigations [3] where we measured the mass of the ground state without use of the cross correlation technique. In the  $0^{++}$  channel the agreement is satisfactory since the ground state wave function is well dominated by the shortest operators like  $(1/2)\text{tr}(\Phi_x^+ U_{x,\mu} \Phi_{x+\hat{\mu}})$ . Mass measurements in the  $2^{++}$  channel and for the  $W$ -ball states have proved to be difficult in our previous studies, and we did not report on that. From the present analysis we recognise that this difficulty is related to the large spatial extendedness of these states.

Using the cross correlation technique we have found in the symmetric phase the ground state mass and the first excitations. We restricted ourselves to an identifications of masses with a still reasonable plateau behaviour and a not too large mass in lattice units. Notice that the classified operators are defined in the angular momentum  $J$  only up to modulo 4, therefore we cannot exclude that too large masses got contributions from states with higher  $J$ .

The first excitations (for  $2^{++}$  only the lowest state) are presented in Fig. 8 and the fitted masses are collected in Tables 2-3 of Appendix A. We tried to illustrate whether

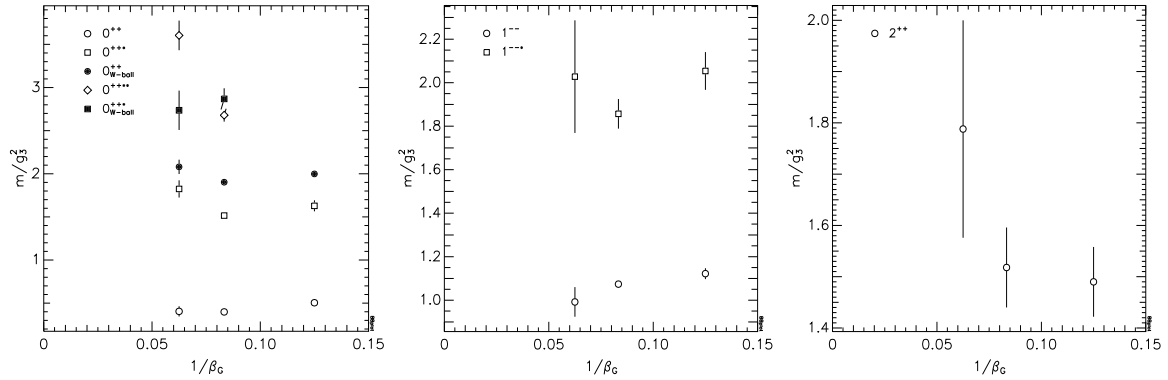


Figure 8: Mass spectrum in the symmetric phase as function of  $1/\beta_G$

the approach to continuum limit is already indicated by the present measurements. The big errors of the excited state in the  $1^{--}$  channel and even more the ground state in the  $2^{++}$  channel show where the problems are.

Concluding this Section we would like to stress that there is no qualitative difference in the spectrum on the high temperature side of the phase transition for light or relatively heavy Higgs masses as long as the phase transition persists. The gauge d.o.f. decouple from the Higgs excitations and form  $W$ -balls as in confined  $3D$  pure  $SU(2)$  gauge theory [21].

## 4 The Spectrum in the Higgs Phase near to the End-point of the Transition

On the Higgs side of the phase transition pure gauge matter  $W$ -ball excitations are not expected to be present in the spectrum. This hypothesis has been numerically verified at light Higgs masses [16]. Now, at  $M_H^* = 70$ , we observe in the Higgs phase near to the transition the following. In the  $1^{--}$  and  $2^{++}$  channels the spectrum looks similar to that in the symmetric phase. This was expected from earlier studies for the  $1^{--}$  channel. Therefore the squared wave functions are not shown explicitly.

Note, that in the  $2^{++}$  channel we have not used operators with pure gauge degrees of freedom. Therefore, we cannot observe the expected difference for  $2^{++}$   $W$ -balls.<sup>1</sup>

In the  $0^{++}$  channel, however, our operator set is sufficient to observe a marked difference between the phases which is not in accordance to simple expectations. As a characteristic feature we observe the mixing between the two operator types,  $W$ -ball operators (with pure gauge d.o.f.) and operators projecting onto Higgs states. The ground state squared wave function looks similar to that in the symmetric phase, contributions from Wilson loops to the operators projecting onto the lowest mass states are absent (Fig. 9). Already the first excited Higgs state contains a noticeable contribution from Wilson

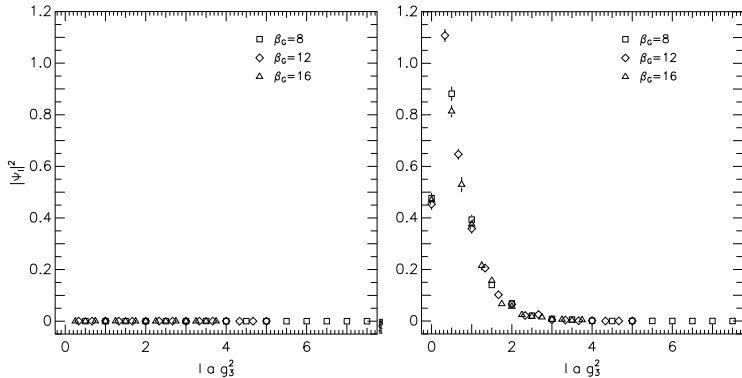


Figure 9: Wave function of the ground state in the  $0^+$  channel, left: Wilson-loops, right: extended operators  $S_{x,\mu}(l)$ ,  $l = 0, \dots, 15$

loop operators of almost 20 percent (Fig. 10). Earlier measurements at a Higgs mass of  $M_H^* = 35$  GeV [17] (where the phase transition is very strong) did not indicate such a mixing. We interpret this mixing of Higgs and gauge d.o.f. as a signal of the near endpoint of the phase transition. Deeper in the Higgs phase the contribution from gauge degrees

<sup>1</sup>Results for the  $W$ -balls with  $J = 2$  can be found in [17].

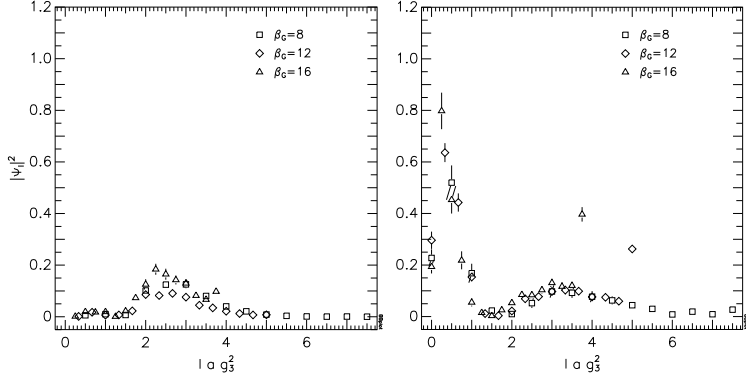


Figure 10: *Same as Fig. 9 for first excitation*

of freedom is expected to disappear also at this high Higgs mass. This tendency has been checked in a simulation at  $M_H^* = 100$  GeV as to be discussed in the next section. This suggests that the first and second excited states present on the symmetric side (Higgs and  $W$ -ball) seem to merge into one common state on the Higgs side. The remaining gauge degrees of freedom are fading with further lowering of temperature (increasing  $\beta_H$ ).

The second excited state in the  $0^{++}$  channel on the Higgs side (Fig. 11) is qualitatively

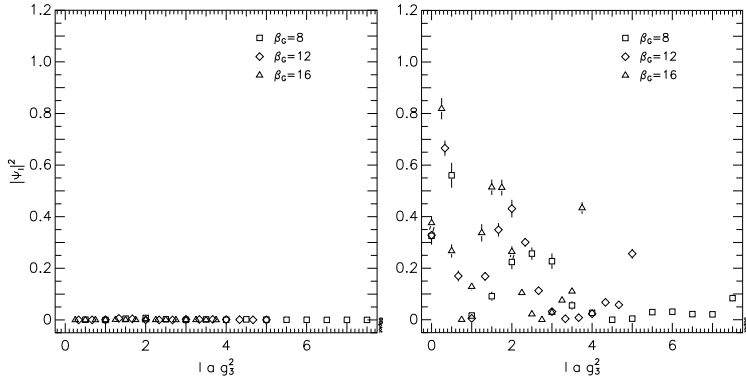


Figure 11: *Same as Fig. 9 for second excitation*

a state with Higgs excitations (no  $W$ -ball contributions) followed by a third excited state which looks dominantly like a  $W$ -ball.<sup>2</sup>

In Fig. 12 our results for the masses at different gauge couplings are collected, the corresponding values can be found in Tables 4 and 5. Similar as before, the lowest mass state has a reasonable continuum limit whereas with increasing mass the accuracy rapidly decreases and an extrapolation to vanishing lattice spacing becomes difficult.

<sup>2</sup>Its wave function is not shown here.

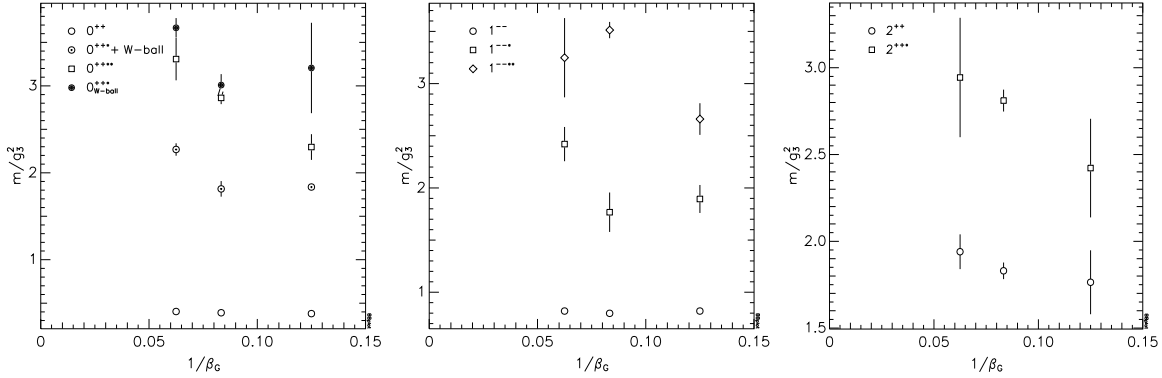


Figure 12:  $\beta_G$  dependence of the spectrum in the Higgs phase

## 5 The Spectral Change along the Rapid Crossover at $M_H^* = 100$ GeV

We have noticed that the spectra of the two phases differ mainly with respect to the contributions of the Wilson loops (gauge d.o.f.) to the excited states in different channels. Therefore we study this change in more detail passing the crossover line changing the hopping parameter  $\beta_H$  at fixed gauge coupling  $\beta_G = 12$ . Sufficiently above the phase transition endpoint (for large enough scalar self-couplings) no large autocorrelation times are expected which would prevent us to go through the region of still rapidly changing observables and determine the correct excitations. As long as a phase transition exists, due to tunnelling one would measure in the  $0^{++}$  not the true spectrum related to the phases but rather a characteristic correlation length characterising the transition itself.

Our simulation have been performed at a scalar–gauge coupling ratio  $\lambda_3/g_3^2 \approx 0.1953$  corresponding to the approximate Higgs mass parameter  $M_H^* = 100$  GeV. We use the same operator set as in the previous analysis. The statistics of 4000 independent configurations per  $\beta_H$  value limits the capability to analyse higher excitations. Nevertheless, we found a behaviour very similar to our results obtained at  $M_H^* = 70$  GeV. The similarities concern the high temperature side of the crossover (similar to the symmetric phase at smaller Higgs mass).

The similarities are in the region where one expects the properties of the symmetric phase and also near the crossover line on the so called Higgs side of the phase diagram. In Figs. 13 we present the spectrum of the lowest states in the  $0^{++}$  channel as function of  $m_3^2(g_3^2)/g_3^4$  ( $\beta_H$ ) over a wide interval above and below the crossover (in temperature).

By inspecting the Figures we identify the crossover position at the position  $m_3^2(g_3^2)/g_3^4 \approx -0.05$ . Of particular interest is for us the  $0^{++}$  channel to study the mixing of Higgs and gauge degrees of freedom. Inspecting the  $0^{++}$  channel of Figs. 13 we conclude that the scalar and gauge sector are approximately decoupled as long as we do not come near to the crossover line from the high temperature side. This has already emphasised in [16, 17] by studying smaller (existence of phase transition) and larger (crossover far away from the endpoint) Higgs self-couplings. The lowest mass  $W$ -ball state (full triangle) is roughly independent of  $\beta_H$  as long as we are not entering into the would-be Higgs phase. On the

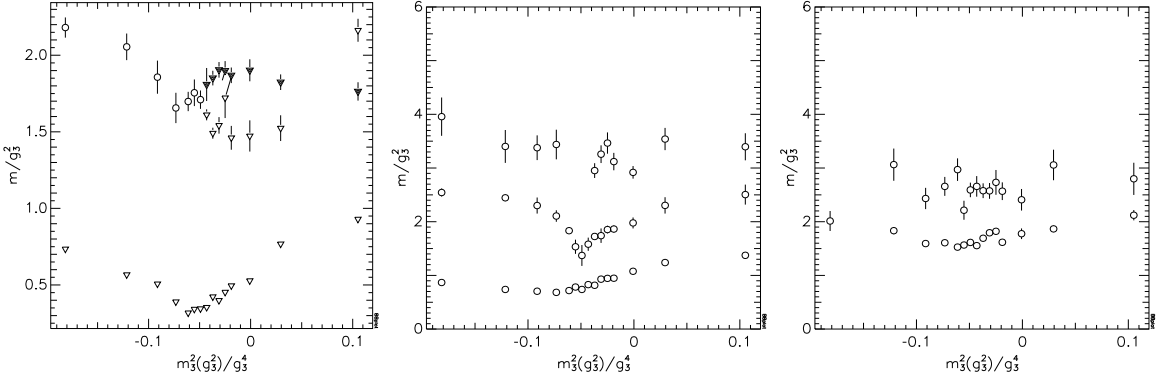


Figure 13: Spectra near the crossover in channels  $0^{++}$ ,  $1^{--}$  and  $2^{++}$ , in the  $0^{++}$  channel open triangles denote Higgs states, full triangles W-ball states and open circles Higgs states with a mixing of gauge d.o.f.

high temperature side of the crossover the spectrum qualitatively resembles very much the spectrum at smaller values of Higgs self-coupling (at  $M_H^* = 70$ ). If we come closer to the crossover line the first Higgs excitation is moving to the  $W$ -ball ground state and at a certain point we observe a growing admixture to this Higgs excitation by contributions from Wilson loop operators which reaches about 17 %. The wave function looks similar to figure 10. At higher  $\beta_H$  (lower temperature, deeper in the would-be Higgs phase) the admixture from pure gauge d.o.f. has disappeared again. This has been explicitly checked for the data point at  $\beta_H = 0.37$ ,  $m_3^2(g_3^2)/g_3^4 \approx -3.4$  given in table 6 (deep in the Higgs-side) in the  $0^{++}$  channel where we do not observe any contribution from the Wilson loops to the first excited state.

## 6 Summary and conclusions

In this paper we complemented our numerical study of the electroweak phase transition using the  $3D$   $SU(2)$ –Higgs model by an investigation of the ground state and excited states in three  $J^{PC}$  channels. Our interest was focused on Higgs screening masses slightly below and above the end of the first order phase transition where we wanted to understand the qualitative relations between the high and lower temperature regions. This investigation was done with help of cross correlations matrix functions between different operators in the same channel. We were able significantly to improve the old ground state mass estimates which were obtained by fitting a single correlations function to the plateau. Earlier the extension of the operators has been chosen by hand, according to a signal *vs.* noise criterion for each channel. Implicitly this procedure gives a hint concerning the best-projecting operator relating the vacuum state to the lowest mass bound state in the given channel. Many techniques are known today which allow to construct source operators with improved projection properties. For the  $SU(2)$ –Higgs and the pure  $SU(2)$  model these are smearing techniques which were investigated and used in our present context in [20, 16, 17]. These improved operators take the extended character of the states into account, too, although in a summary way.

Using the cross correlation technique the extended character can be specified in a more detailed and systematic way. Within a preselected set of operators, the method finds the projection strength of each operator onto the first few states with quantum numbers compatible to the operators admitted. The result can be represented as a wavefunction. Moreover, different Fock space components (Higgs bound states and gauge-ball states) can be treated in parallel. In the present paper this feature has been proven essential for the understanding of excited states and to point out similarities and differences between neighbouring regions of the extended phase diagram. Our operators were classified in a very simple way (extended Higgs links and Wilson loops without internal structure) with clear reference to the corresponding length in lattice units.

This allows us to interpret the results in terms of a configuration space wave function. With this in mind and to do a first step our operator choice was just the simplest one to incorporate the notion of spatial extension. It was possible to see the particular effects that typically occur when the admitted operator set gets too small (in attempts to go too far to the continuum limit  $a \rightarrow 0$ ) to cover the state under discussion. The continuum limit of the screening masses and wave functions has to be accompanied by correspondingly larger lattices with the same physical volume. Plainly increasing the operator set simultaneously would require much higher statistics to reach the necessary accuracy and stability in the diagonalisation procedure. This is a reason to include, in a next step of improvement of the method, smearing of the fields in the operators and/or the construction of blocked operators.

Our first measurements are done at a Higgs mass of  $M_H^* = 70$  GeV near the endpoint of the transition. We found that the physics at this point is already influenced by the endpoint. The  $W$ -ball states of the symmetric phase do not disappear in the Higgs phase as long as one keeps near to the transition line. However, the first  $W$ -ball state appears as an admixture in the first excited Higgs state. A second  $W$ -ball state could also be seen in the Higgs phase very near to the phase transition.

Our measurements in the crossover region have shown that also there the  $W$ -ball state will disappear deeper on the low temperature side of the crossover. With the simulations at  $M_H^* = 100$  GeV we could indicate a mixing of the first  $W$ -ball with the first Higgs excited state in more detail by following the spectral evolution across the crossover line. The decoupling of the gauge and scalar sector was proven over most of the parameter space on the high temperature side of the crossover region.

## A Tables of fitted measured masses for ground states and excitations

$\beta_G$	$\beta_H$	$0^{++}$	$0^{++*}$	$0_{W\text{-ball}}^{++}$	$0^{++**}$	$0_{W\text{-ball}}^{++*}$
8	0.3490	0.504(16)	1.628(64)	1.998(37)		
12	0.3434	0.398(18)	1.515(33)	1.902(26)	2.679(75)	2.868(123)
16	0.3407	0.404(59)	1.824(100)	2.080(83)	3.604(172)	2.736(228)

Table 2:  $0^{++}$  mass spectrum for the symmetric phase in units  $g_3^2$ ,  $30^3$  lattice

$\beta_G$	$\beta_H$	$1^{--}$	$1^{--*}$	$2^{++}$
8	0.3490	1.122(35)	2.054(87)	1.498(68)
12	0.3434	1.074(14)	1.857(68)	1.518(78)
16	0.3407	0.992(68)	2.028(259)	1.788(21)

Table 3:  $1^{--}$  and  $2^{++}$  mass spectrum in the symmetric phase in units  $g_3^2$ ,  $30^3$  lattice

$\beta_G$	$\beta_H$	$0^{++}$	$0^{++*} + \text{gauge d.o.f.}$	$0_{W\text{-ball}}^{++}$	$0^{++**}$
8	0.34970	0.380(4)	1.836(36)	2.296(148)	3.206(519)
12	0.34368	0.390(3)	1.815(90)	2.862(71)	3.009(126)
16	0.34088	0.404(4)	2.268(71)	3.308(244)	3.668(112)

Table 4:  $0^{++}$  mass spectrum in the Higgs phase in units  $g_3^2$ ,  $30^3$  lattice

$\beta_G$	$\beta_H$	$1^{--}$	$1^{--*}$	$2^{++}$	$2^{++*}$
8	0.34970	0.820(8)	1.894(134)	1.764(184)	2.422(288)
12	0.34368	0.798(6)	1.767(189)	1.830(48)	2.811(63)
16	0.34088	0.820(12)	2.420(151)	1.940(100)	2.944(344)

Table 5:  $1^{--}$  and  $2^{++}$  mass spectrum in the Higgs phase in units  $g_3^2$ ,  $30^3$  lattice

	$\beta_H$	$0^{++}$	$0^{++*}$	$0_{W\text{-ball}}^{++}$
symmetric side	0.34200	2.037(51)	3.330(225)	1.770(59)
	0.34510	0.930(18)	2.163(75)	1.764(59)
	0.34560	0.768(12)	1.525(84)	1.824(51)
	0.34580	0.528(14)	1.473(102)	1.902(71)
	0.34592	0.495(14)	1.461(78)	1.869(51)
	0.34596	0.453(14)	1.722(131)	1.899(63)
	0.34600	0.399(53)	1.542(53)	1.905(51)
	0.34604	0.423(14)	1.491(35)	1.851(48)
	0.34608	0.354(12)	1.611(35)	1.809(107)
		$0^{++}$	$0^{++*} + \text{gauge d.o.f.}$	
Higgs side	0.34612	0.345(6)	2.316(248)	
	0.34616	0.342(12)	2.679(164)	
	0.34628	0.390(6)	2.841(180)	
	0.34640	0.507(6)	2.565(239)	
	0.34660	0.567(12)	3.147(246)	
	0.34700	0.735(9)	2.982(282)	
		$0^{++}$	$0^{++*}$	$0^{++**}$
	0.37000	2.723(48)	5.250(339)	5.220(210)

Table 6:  $0^{++}$  spectrum at  $M_H^* = 100$  GeV in units  $g_3^2$

	$\beta_H$	$1^{--}$	$1^{--*}$	$1^{--**}$	$2^{++}$	$2^{++*}$
symmetric side	0.34200	2.037(51)	3.330(225)	1.770(59)	3.255(84)	4.086(210)
	0.34510	1.374(48)	2.505(185)	3.396(252)	2.121(96)	2.799(300)
	0.34560	1.239(30)	2.304(152)	3.540(206)	1.866(63)	3.057(284)
	0.34580	1.077(14)	1.977(102)	2.919(116)	1.776(98)	2.409(201)
	0.34592	0.948(21)	1.863(68)	3.120(162)	1.670(35)	2.568(164)
	0.34596	0.945(21)	1.854(71)	3.465(197)	1.821(53)	2.733(231)
	0.34600	0.930(12)	1.740(135)	3.258(164)	1.794(51)	2.574(147)
	0.34604	0.816(35)	1.725(59)	2.952(137)	1.692(45)	2.577(137)
	0.34608	0.828(26)	1.581(123)		1.554(51)	2.658(192)
Higgs side	0.34612	0.738(24)	1.371(194)		1.614(29)	2.592(135)
	0.34616	0.783(17)	1.533(132)		1.566(42)	2.214(177)
	0.34620	0.717(32)	1.833(60)		1.527(42)	2.970(210)
	0.34628	0.684(21)	2.106(107)	3.438(275)	1.608(44)	2.658(177)
	0.34640	0.705(26)	2.301(150)	3.378(231)	1.593(56)	2.433(197)
	0.34660	0.738(24)	2.445(63)	3.402(305)	1.833(65)	3.063(300)
	0.34700	0.867(12)	2.544(75)	3.957(357)	2.013(185)	
	0.37000	0.800(11)	1.915(70)			

Table 7:  $1^{--}$  and  $2^{++}$  spectrum at  $M_H^* = 100$  GeV in units  $g_3^2$

## B Angular Momentum in 2+1 Dimensions

Gauge invariant operators can be constructed in the 3D  $SU(2)$ –Higgs model and can be used to define states and wave functions. They are classified with respect to the quantum numbers angular momentum  $J$ , parity  $P$  and charge conjugation  $C$ . While the classification according to  $C$  and  $P$  is trivial (the eigenvalues of  $C$  and  $P$  have the same sign for operators which live in the same  $x - y$ -plane in 2+1 dimensions) the classification according to  $J$  requires some care due to the discreteness of the rotation group. The results are known, we collect here the main results for the convenience of the reader and to apply them to the operators of interest. For the 3+1 dimensional case the classification can be found in [22, 23]. Some of the results are already described in [24], we follow the description in [25].

To define the angular momentum of a given operator on the lattice the transformation properties with respect to the discrete lattice symmetries have to be studied. In our case the continuous symmetry group is  $SO(2)$  which gets restored in the continuum limit. In that case the angular momentum is represented by the irreducible representations (IR) of  $SO(2)$ . On the cubic lattice the group of two-dimensional rotations and reflections is the dihedral group  $\mathcal{D}_4$ . This group is nonabelian and has 8 elements ( $d = 8$ ) and 5 irreducible representations. The conjugation classes  $C$  with their number of elements  $n_C$  and the symmetry transformations are collected in Table 8. The corresponding IR's of

$C(n_C)$	angle	
$\mathbf{1}(1)$	Identity	
$C_4^2(1)$	rotation (0,0)	$\phi = \pi$
$C_4(2)$	rotation (0,0)	$\phi = \pi/2$
$C_2(2)$	reflection x, y	
$C'_2(2)$	reflection diagonal	

Table 8: Symmetry transformations of  $\mathcal{D}_4$  group

$\mathcal{D}_4$  are denoted by  $A_1$ ,  $A_2$ ,  $B_1$ ,  $B_2$  and  $E$ , the first four are one-dimensional, the last one has dimension 2.

The characters of  $\mathcal{D}_4$  are computed by reducing the characters of the full  $SO(2)$  group (including reflections) (table 9) to those of the subduced representation  $D_0^J$  by taking the discrete angles of table 8. The result is shown in table 10. The characters of the conjugation classes of  $\mathcal{D}_4$  in the IR of this group are taken from the character table of [25] and shown in table 11. Using the characters given in tables 10 and 11 we can compute the multiplicities for the IR of the dihedral group  $\mathcal{D}_4$  for angular momentum  $J$ :

$$m_J^{IR} = \frac{1}{d} \sum_C n_C \chi_C^{IR} \chi_C^J, \quad (16)$$

they are shown in table 12.

The multiplicities for a given operator are obtained by inspecting its properties under those discrete transformations. The extended operators (given in (12)) transform as

$C_\infty \setminus J$	0	1	2	3	4
<b>1</b>	1	2	2	2	2
$C(\phi)$	1	$2\cos\phi$	$2\cos 2\phi$	$2\cos 3\phi$	$2\cos 4\phi$
$\sigma_v$	1	0	0	0	0

Table 9: Characters  $\chi^J$  of full  $SO(2)$  symmetry ( $C(\phi)$ ) including reflections ( $\sigma_v$ ) for various angular momenta  $J$

$C \setminus J$	0	1	2	3	4
<b>1(1)</b>	1	2	2	2	2
$C_4^2(1)$	1	-2	2	-2	2
$C_4(2)$	1	0	-2	0	2
$C_2(2)$	1	0	0	0	0
$C'_2(2)$	1	0	0	0	0

Table 10: Characters  $\chi_C^J$  of conjugation classes  $C$  in the subduced representation  $D_0^J$

$C \setminus IR$	$A_1$	$A_2$	$B_1$	$B_2$	$E$
<b>1(1)</b>	1	1	1	1	2
$C_4^2(1)$	1	1	1	1	-2
$C_4(2)$	1	1	-1	-1	0
$C_2(2)$	1	-1	1	-1	0
$C'_2(2)$	1	-1	-1	1	0

Table 11: Characters  $\chi_C^{IR}$  of the conjugation class  $C$  in the IR of  $\mathcal{D}_4$

$J \setminus IR$	$A_1$	$A_2$	$B_1$	$B_2$	$E$
0	1	0	0	0	0
1	0	0	0	0	1
2	0	0	1	1	0
3	0	0	0	0	1
4	1	1	0	0	0

Table 12: Multiplicities  $m_J^{IR}$  of IR of  $\mathcal{D}_4$  in the subduced representation  $D_0^J$  for angular momentum  $J$

vectors with positive parity ( $S_{x,\mu}(l)$ ) or with negative parity ( $V_{x,\mu}^b(l)$ ). The characters and the multiplicities are shown in table 13. We observe that the operator  $S_{x,\mu}(l)$  transforms

		<b>1(1)</b>	$C_4^2(1)$	$C_4(2)$	$C_2(2)$	$C'_2(2)$		$A_1$	$A_2$	$B_1$	$B_2$	$E$
$S_{x,\mu}(l)$	$\chi_C^{IR}$	2	2	0	2	0	$m_J^R$	1	0	1	0	0
$V_{x,\mu}^b(l)$	$\chi_C^{IR}$	2	-2	0	0	0	$m_J^R$	0	0	0	0	1

Table 13: Characters and multiplicities for the operators  $S_{x,\mu}(l)$  and  $V_{x,\mu}^b(l)$

simultaneously under the IR  $A_1$  and  $B_1$ , whereas  $V_{x,\mu}^b(l)$  transforms with  $E$  only.

Using a projection operator  $P^{IR}$  one is able to project onto *one* irreducible representation in the case of  $S_{x,\mu}(l)$ . A projection operator for a given IR is constructed as the sum over all conjugation classes  $C$  weighted by the character  $\chi_C^{IR}$  for that IR (table 11):

$$P^{IR} = \sum_C \chi_C^{IR} C. \quad (17)$$

The  $C$  have to be taken in a matrix representation taking into account parity.

For the operator  $S_{x,\mu}(l)$  the projection matrices can be used in the form:

$$P^{A_1} = 4 \begin{pmatrix} 1 & 1 \\ 1 & 1 \end{pmatrix}, \quad P^{B_1} = 4 \begin{pmatrix} 1 & -1 \\ -1 & 1 \end{pmatrix}. \quad (18)$$

$0^{++}$ :	$S_{x,1}(l) + S_{x,2}(l)$
	$W_{x,1,2}(l) + W_{y,1,2}(l)$
$1^{--}$ :	$V_{x,1}^b(l) + V_{x,2}^b(l)$
$2^{++}$ :	$S_{x,1}(l) - S_{x,2}(l)$
	$W_{x,1,2}(l) - W_{y,1,2}(l)$

Table 14: Quantum numbers and gauge invariant lattice operators

From here the fixed angular momenta of the operators to be used are defined as shown in table 14. It is obvious from table 12 that all operators describing a  $J = 0$  angular momentum state also overlap to a  $J = 4$  state. These higher states are expected to be sufficiently heavier than the lightest  $J = 0$  state. Similarly this also holds for the other operators. Thus for the cubic lattice only operators with  $J(\text{mod } 4)$  can be constructed what restricts the identification of highly excited states in the channels discussed here.

## References

- [1] K. Kajantie *et al.*: Nucl. Phys. **B442** (1995) 317; **B466** (1996) 189
- [2] F. Karsch *et al.*: Nucl. Phys. **B474** (1996) 217
- [3] M. Gürler *et al.*: Nucl. Phys. **B483** (1997) 383
- [4] K. Kajantie, M. Laine, K. Rummukainen and M. Shaposhnikov: Phys. Rev. Lett. **77** (1996) 2887
- [5] M. Gürler, E.-M. Ilgenfritz, and A. Schiller: Phys. Rev. **D56** (1997) 3888
- [6] M. Gürler, E.-M. Ilgenfritz, A. Schiller: Eur. Phys. J. **C 1** (1998) 363
- [7] Z. Fodor *et al.*: Nucl. Phys. **B439** (1995) 147; F. Csikor *et al.*: Nucl. Phys. **B474** (1996) 421; Y. Aoki: Phys. Rev. **D56** (1997) 3860; F. Csikor, Z. Fodor, J. Heitger: Nucl. Phys. **B (Proc. Suppl.) 63** (1998) 569
- [8] K. Rummukainen: Nucl. Phys. **B (Proc. Suppl.) 53** (1997) 30
- [9] K. Kajantie, M. Laine, K. Rummukainen, and M. Shaposhnikov: Nucl. Phys. **B458** (1996) 90
- [10] M. Laine: Nucl. Phys **B451** (1995) 484
- [11] K. Rummukainen *et al.*: preprint CERN-TH-98-08, hep-lat/9805013.
- [12] S. de Jong: “*Higgs Searches at LEP*”, Review talk delivered at the XXXIIIrd Rencontres de Moriond, Les Arcs, France, March 14 – 21 (1998) .

- [13] M. Laine, K. Rummukainen: Phys. Rev. Lett. **80** (1998) 5259; CERN-TH-98-122, hep-lat/9804019
- [14] M.N. Chernodub, F.V. Gubarev, E.-M. Ilgenfritz, A. Schiller: ITEP-TH-12/98, KANAZAWA-98-03 and ZIF-MS-30/98 preprint, hep-lat/9805016, to appear in Phys. Lett. **B**; ITEP-TH-36/98, KANAZAWA-98-08 and UL-NTZ 30/98 preprint, hep-lat/9807016;
- [15] M. Gürtler, E.-M. Ilgenfritz, A. Schiller, and C. Strecha: Nucl. Phys. **B (Proc. Suppl.) 63** (1998) 563; HUB-EP-98/05 and KANAZAWA 98-01 preprint, hep-lat/9801012
- [16] O. Philipsen, M. Teper, and H. Wittig: Nucl. Phys. **B469** (1996) 445
- [17] O. Philipsen, M. Teper, and H. Wittig: hep-lat/9709145, to appear in Nucl. Phys. **B**
- [18] M. Lüscher and U. Wolff: Nucl. Phys. **B339** (1990) 222
- [19] C.R. Gattringer, C.B. Lang: Nucl. Phys. **B391** (1993) 463
- [20] M. Teper: Phys. Lett. **B187** (1987) 345
- [21] M. Teper: Phys. Lett. **B311** (1993) 223
- [22] B. Berg, A. Billoire: Nucl.Phys. **B221** (1983) 109 ; K. Ishikawa, G. Schierholz, M. Teper: Z. Phys. **C19** (1983) 327
- [23] H.G. Evertz: "Gitteranalyse des Higgs-Mechanismus", Dissertation TH Aachen RX-1200 (1987)
- [24] V. Agostini, G. Carlino, M. Caselle, M. Hasenbusch: Nucl. Phys. **B484** (1997) 331
- [25] M. Hamermesh: "Group theory and its application to physical problems ", New York: Dover Publications 1989